Electronic Supplementary Material (ESI) for Materials Advances.

Supplementary Information

Investigation of the influence of Natural Deep Eutectic Solvents (NaDES) in the properties of chitosan-stabilised films.

Antonella Rozaria Nefeli Pontillo [a], Spyridon Koutsoukos[b], Tom Welton[b] and Anastasia Detsi*[a]

[1] Laboratory of Organic Chemistry, Department of Chemical Sciences, School of Chemical Engineering, National Technical University of Athens, Zografou, Greece
[2] Department of Chemistry, Molecular Sciences Research Hub, Imperial College London, White City Campus, London W12 0BZ, UK.

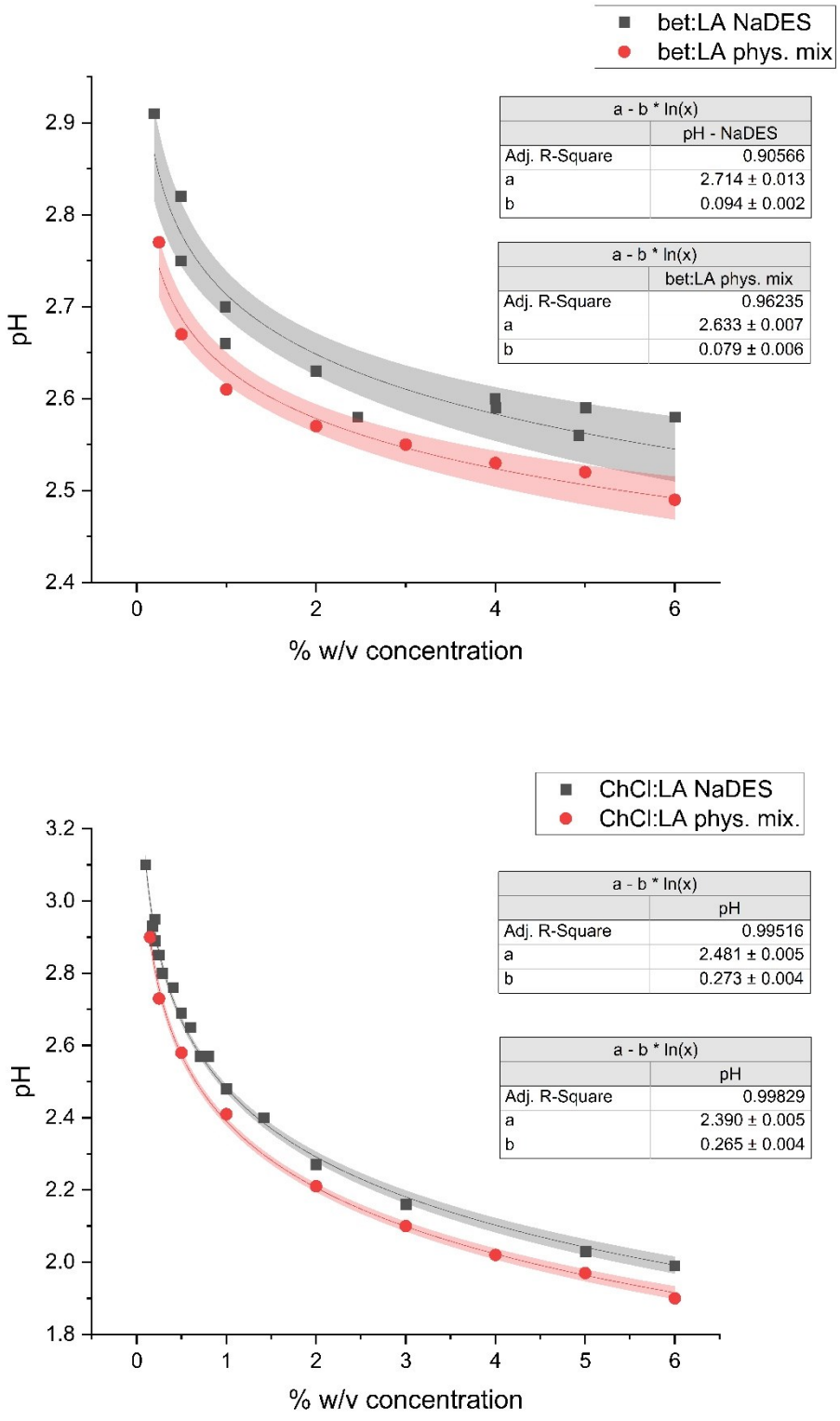

Figure S1. Curve of pH Vs concentration of the bet:LA NaDES and physical mixture (top) and the ChCl:LA NaDES and physical mixture (bottom).

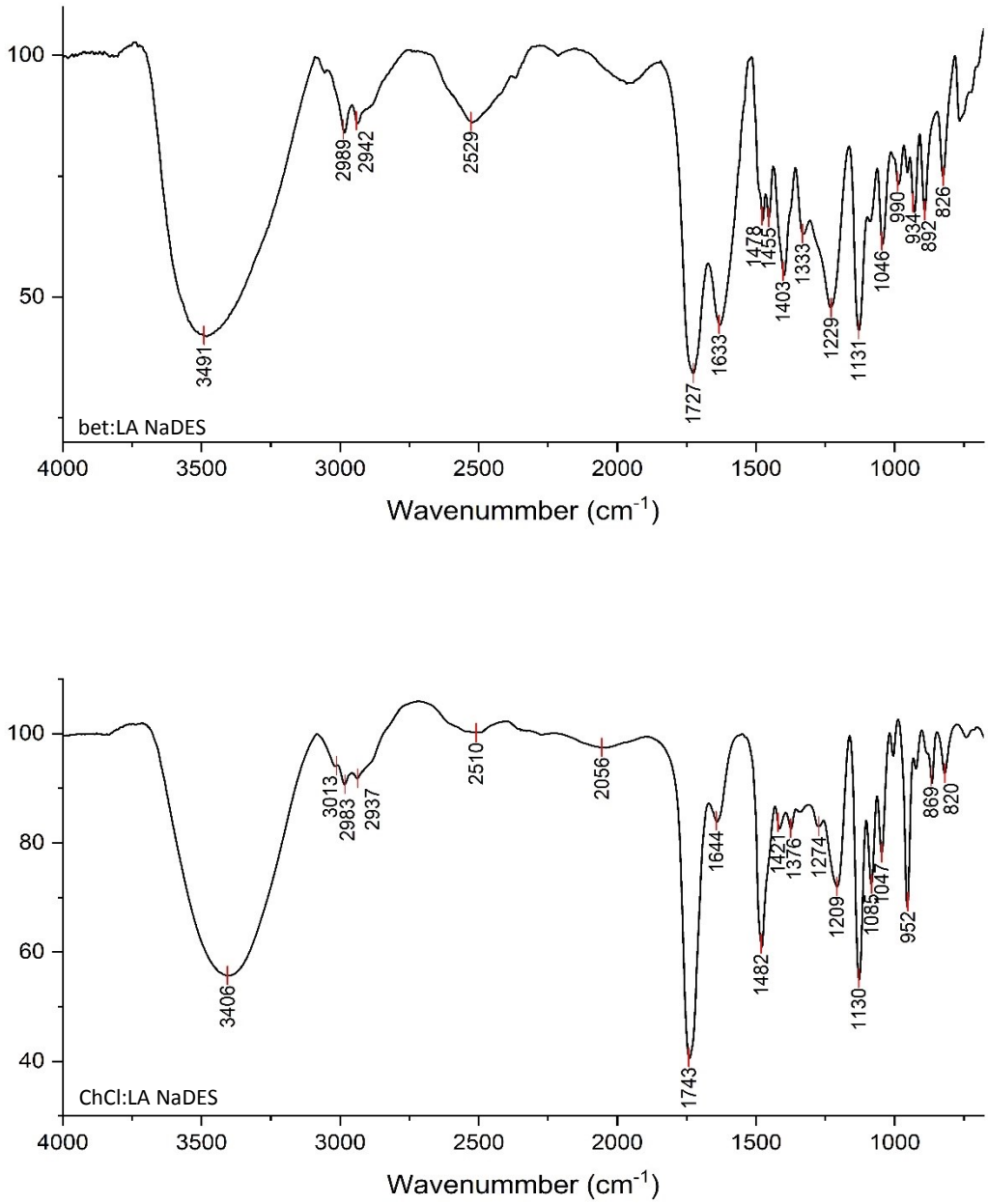

Figure S2**.** FT-IR spectra of the bet:LA NaDES (top) and the ChCl:LA NaDES (bottom).

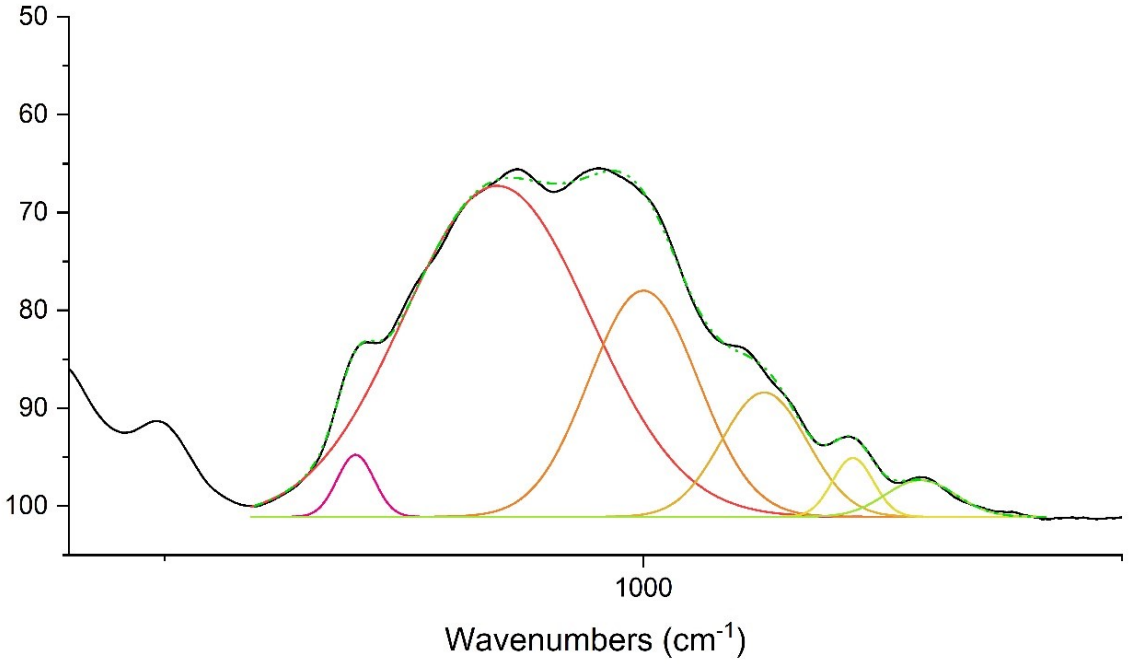

Figure S3. Deconvolution of 1200-840 cm^{-1} range for F/AA.

Table S1. Accuracy of deconvolution model for F/AA.

Model	Gauss					
Equation	$y = y_0 + \left(\frac{A}{w * \sqrt{\frac{\pi}{2}}}\right) * e^{\left(-2 * \left(\frac{x - x_c}{w}\right)^2\right)}$					
	Peak 1	Peak 2	Peak 3	Peak 4	Peak 5	Peak 6
y_0	101.1 ± 0.1					
x_c	1150.2 ± 0.1	1076.4 ± 0.3	999.9 ± 0.2	936.8 ± 0.3	890 ± 0.2	855.2 ± 0.6
W	19.3 ± 0.2	97.2 ± 0.5	57.0 ± 0.5	45.1 ± 0.6	21.4 ± 0.5	36.6 ± 1.1
A	-153 ± 3	-4122 ± 31	-1650 ± 32	-719 ± 15	-161 ± 6	-172 ± 6
R-Square	0.99929					
Adj. R-Square	0.99928					

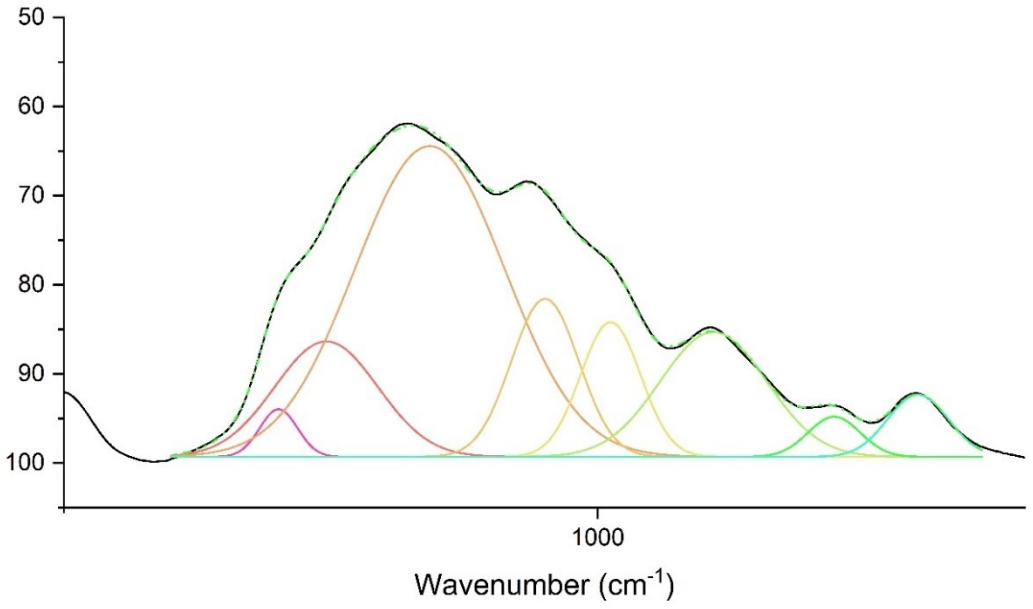

Figure S4. Deconvolution of 1200-840 cm^{-1} range for F/Tween.

Table S2. Accuracy of deconvolution model for F/Tween.

Model	Gauss							
Equation	$y = y_0 + \left(\frac{A}{w * \sqrt{\frac{\pi}{2}}}\right) * e^{\left(-2 * \left(\frac{x - x_c}{w}\right)^2\right)}$							
	Peak 1	Peak 2	Peak 3	Peak 4	Peak 5	Peak 6	Peak 7	Peak 8
y_0	99.31 ± 0.05							
x_c	1149.4 ± 0.1	1127 ± 2	1079 ± 2	1024.7 ± 0.3	994 ± 0.3	945.9 ± 0.2	889.3 ± 0.2	850.1 ± 0.1
W	17.7 ± 0.2	48.3 ± 2.6	69.9 ± 5.6	31.6 ± 0.8	28.2 ± 0.4	49.8 ± 0.4	24.5 ± 0.4	28.4 ± 0.3
A	-118 ± 3	-784 ± 27	-3056 ± 349	-702 ± 65	-534 ± 16	-874 ± 8	-138± 3	-249 ± 4
R-Square	0.99974							
Adj. R-Square	0.99974							

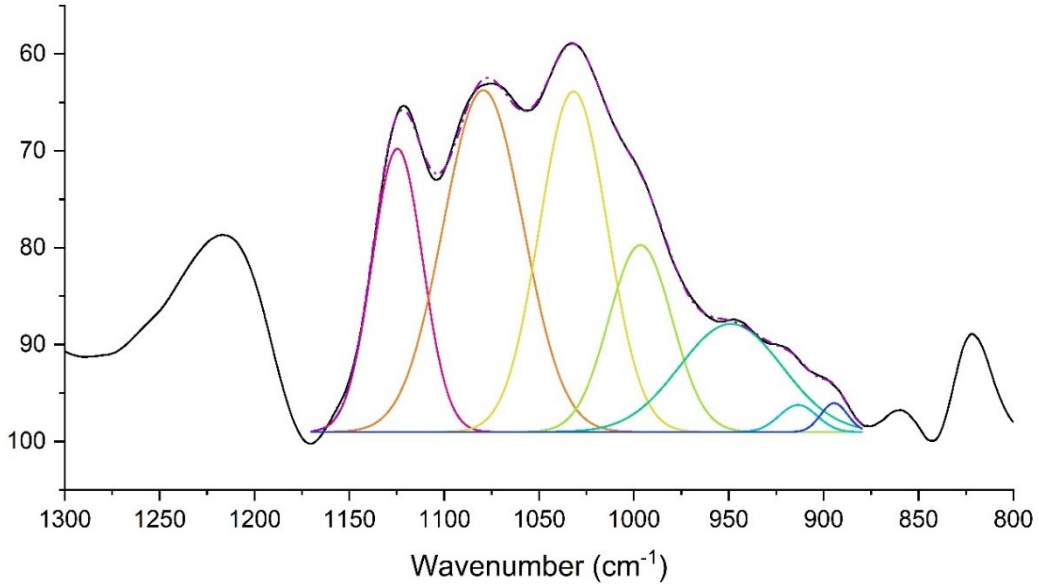

Figure S5. Deconvolution of 1200-840 cm^{-1} range for F/0.5LA.

Table S3. Accuracy of deconvolution model for F/0.5LA.

Model	Gauss						
Equation	$y = y_0 + \left(\frac{A}{w * \sqrt{\frac{\pi}{2}}}\right) * e^{\left(-2 * \left(\frac{x - x_c}{w}\right)^2\right)}$						
	Peak 1	Peak 2	Peak 3	Peak 4	Peak 5	Peak 6	Peak 7
y_0	99.0 ± 0.1						
x_c	1124.7 ± 0.1	1079.4 ± 0.3	1031.4 ± 0.4	996.6 ± 0.6	948 ± 1	913.5 ± 0.8	894.5 ± 0.6
W	26.6 ± 0.1	42.2 ± 0.6	35.7 ± 0.9	33.3 ± 1.2	54.2 ± 4.5	19.8 ± 2	14.1 ± 1
A	-975 ± 10	-1865 ± 36	-1574 ± 77	-805 ± 87	-758 ± 69	-70 ± 19	-52.9 ± 8.9
R-Square	0.99939						
Adj. R-Square	0.99938						

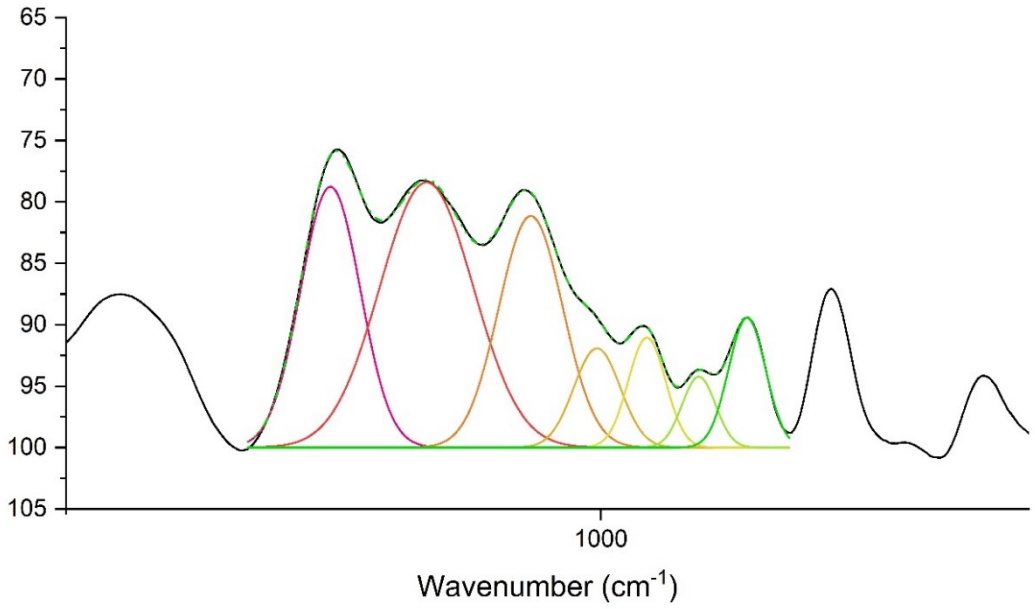

Figure S6. Deconvolution of 1200-920 cm^{-1} range for F/bet:LA.

Table S4. Accuracy of deconvolution model for F/bet:LA.

Model	Gauss						
Equation	$y = y_0 + \left(\frac{A}{w * \sqrt{\frac{\pi}{2}}}\right) * e^{\left(-2 * \left(\frac{x - x_c}{w}\right)^2\right)}$						
	Peak 1	Peak 2	Peak 3	Peak 4	Peak 5	Peak 6	Peak 7
y_0	100 ± 0						
x_c	1126.4 ± 0.1	1081.5 ± 0.1	1032.8 ± 0.1	1001.8 ± 0.1	978.5 ± 0.1	954.3 ± 0.1	931.7 ± 0.1
W	27.9 ± 0.1	43.7 ± 0.3	29.9 ± 0.3	21.8 ± 0.5	17.5 ± 0.3	15.6 ± 0.3	17.3 ± 0.1
A	-743 ± 4	-1181 ± 8	-706 ± 9	-220 ± 8	-196 ± 5	-113 ± 2	-229.1 ± 1
R-Square	0.99959						
Adj. R-Square	0.99959						

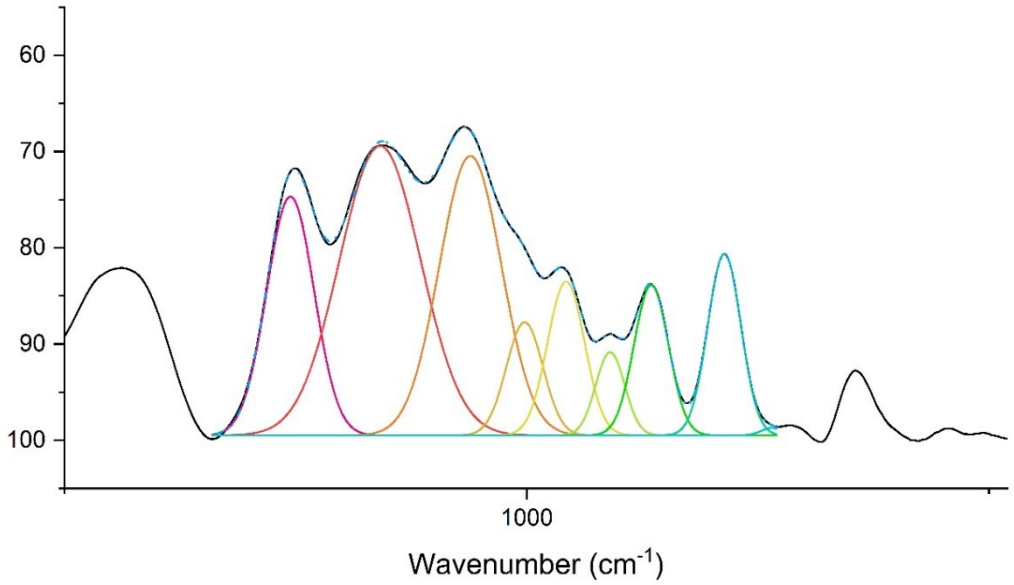

Figure S7. Deconvolution of 1200-840 cm^{-1} range for F/bet:LA mix.

Table S5. Accuracy of deconvolution model for F/bet:LA phys. mix.

Model	Gauss							
Equation	$y = y_0 + \left(\frac{A}{w * \sqrt{\frac{\pi}{2}}}\right) * e^{\left(-2 * \left(\frac{x - x_c}{w}\right)^2\right)}$							
	Peak 1	Peak 2	Peak 3	Peak 4	Peak 5	Peak 6	Peak 7	Peak 8
y_0	100 ± 0							
x_c	1127.7 ± 0.0	1079.3 ± 0.1	1030.5 ± 0.1	1001.1 ± 0.2	978.7 ± 0.2	954.9 ± 0.1	932.7 ± 0.1	893.1 ± 0.1
w	25.6 ± 0.1	43.9 ± 0.3	33.7 ± 0.3	19.8 ± 0.5	20.0 ± 0.4	15.7 ± 0.3	18.6 ± 0.1	17.9 ± 0.1
A	-762 ± 4	-1654 ± 10	-1125 ± 15	-292 ± 14	-401 ± 12	-170 ± 5	-364 ± 3	-424 ± 1
R-Square	0.99971							
Adj. R-Square	0.99971							

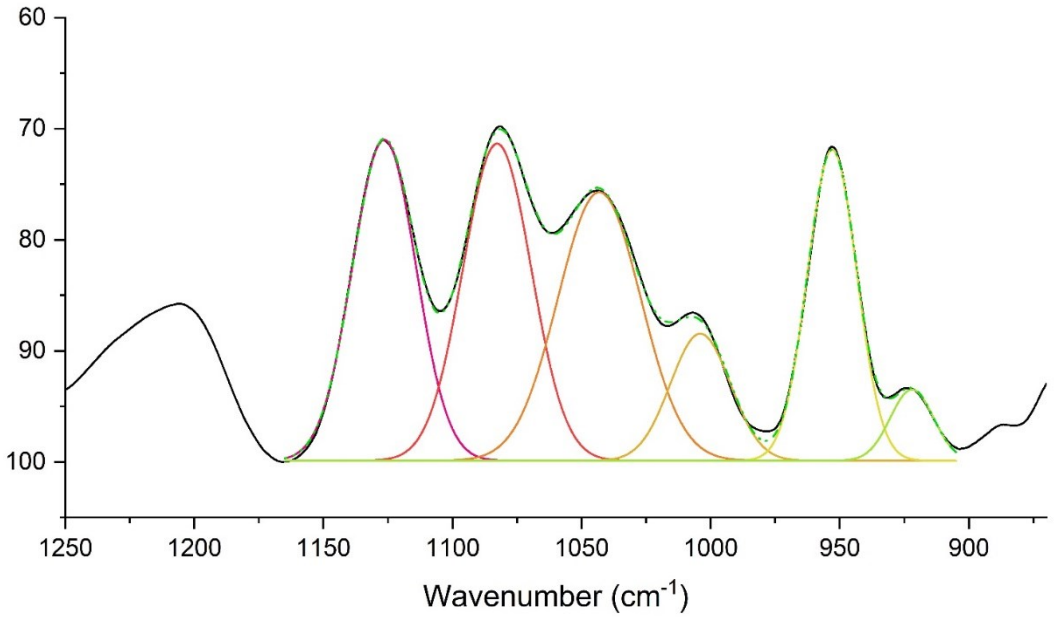

Figure S8. Deconvolution of 1200-840 cm^{-1} range for F/ChCl:LA.

Table S6. Accuracy of deconvolution model for F/ChCl:LA .

Model	Gauss					
Equation	$y = y_0 + \left(\frac{A}{w * \sqrt{\frac{\pi}{2}}}\right) * e^{\left(-2 * \left(\frac{x - x_c}{w}\right)2\right)}$					
	Peak 1	Peak 2	Peak 3	Peak 4	Peak 5	Peak 6
y_0	100 ± 0					
x_c	1126.5 ± 0.0	1082.8 ± 0.1	1043.2 ± 0.0	1004.0 ± 0.0	952.9 ± 0.0	922.1 ± 0.1
w	24.6 ± 0.1	26.5 ± 0.1	32.1 ± 0.2	23.2 ± 0.2	19.1 ± 0.0	16.6 ± 0.2
A	-891 ± 3	-948 ± 5	-972 ± 7	-333 ± 4	-669 ± 2	-134 ± 2
R-Square	0.99921					
Adj. R-Square	0.99920					

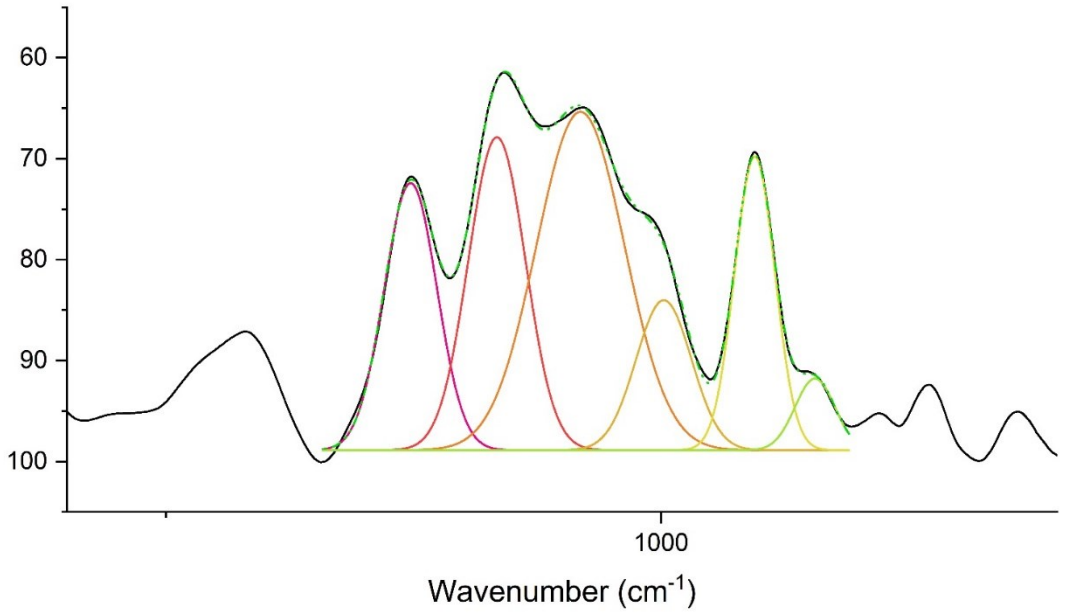

Figure S9. Deconvolution of 1200-840 cm^{-1} range for F/ChCl:LA mix.

Table S7. Accuracy of deconvolution model for F/ChCl:LA mix.

Model	Gauss					
Equation	$y = y_0 + \left(\frac{A}{w * \sqrt{\frac{\pi}{2}}}\right) * e^{\left(-2 * \left(\frac{x - x_c}{w}\right)2\right)}$					
	Peak 1	Peak 2	Peak 3	Peak 4	Peak 5	Peak 6
y_0	98.9 ± 0					
x_c	1126.5 ± 0.0	1082.8 ± 0.1	1040.7 ± 0.1	998.6 ± 0.3	952.7 ± 0.0	922.2 ± 0.1
w	26.6 ± 0.1	28.9 ± 0.2	44.4 ± 0.9	28.0 ± 0.3	20.4 ± 0.1	20.1 ± 0.3
A	-883 ± 5	-1123 ± 23	-1865 ± 39	-522 ± 19	-744 ± 3	-179 ± 3
R-Square	0.99905					
Adj. R-Square	0.99903					

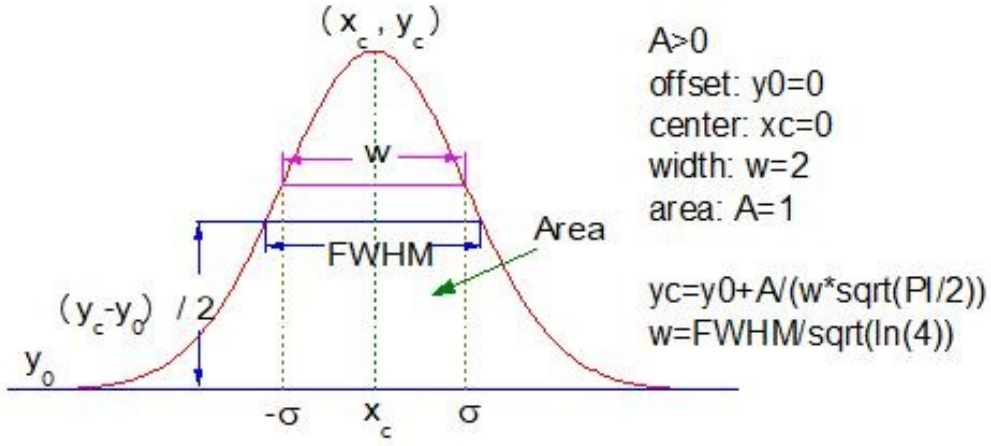

Figure S10. Gauss Curve equation parameters explanation.

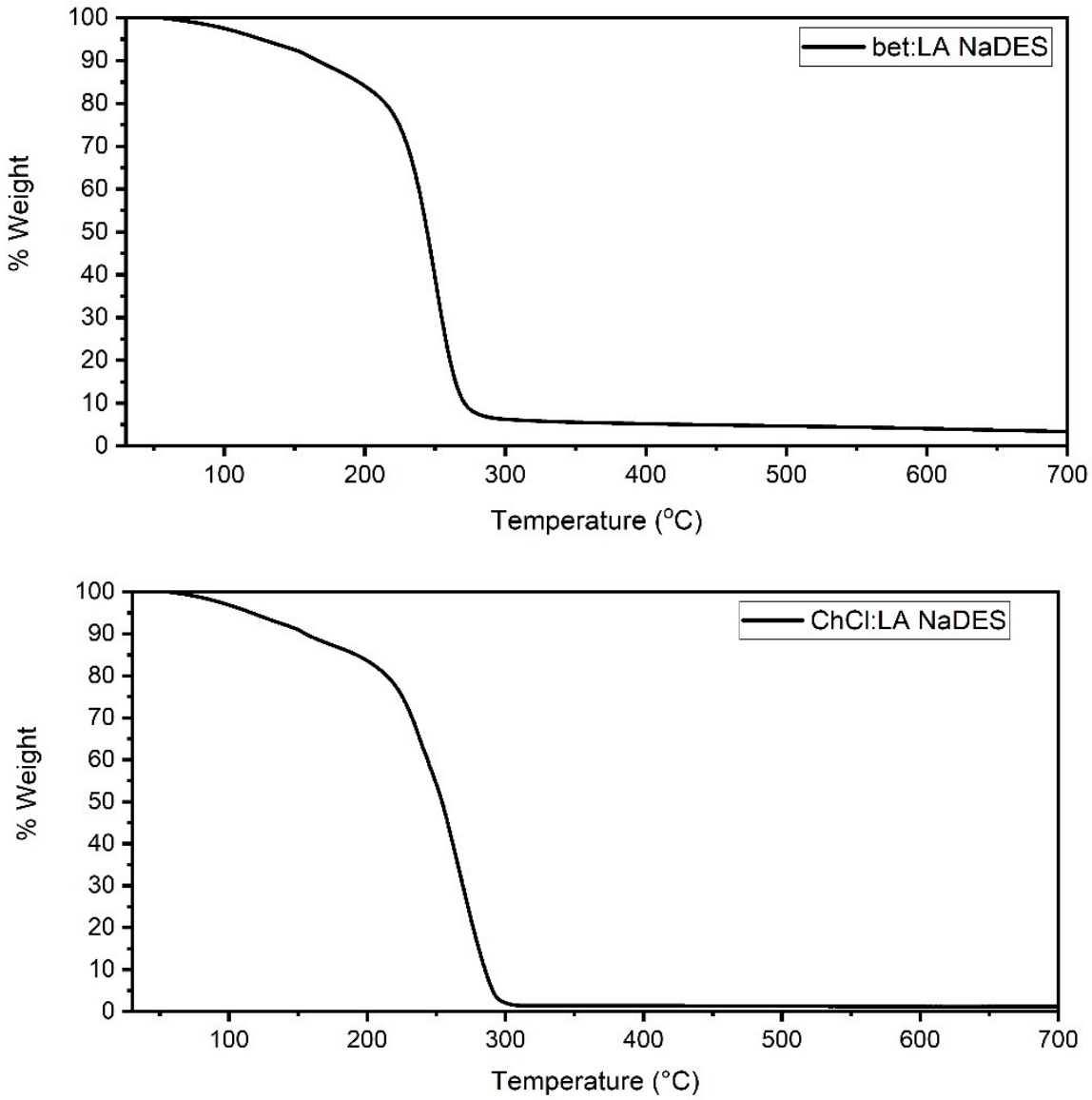

Figure S11. TGA graphs of the bet:LA NaDES (top) and the ChCl:LA NaDES (down).

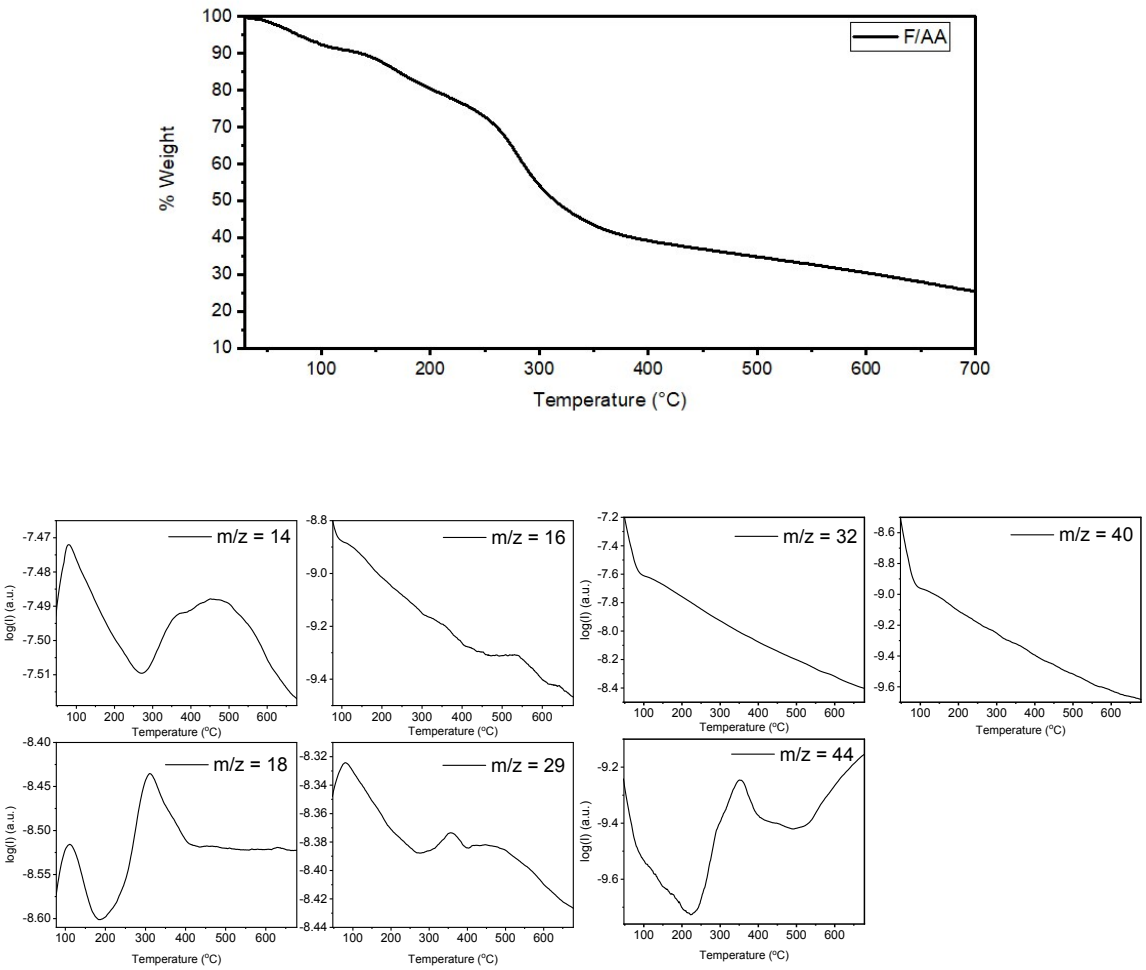

Figure S12. TGA-MS of F/AA.

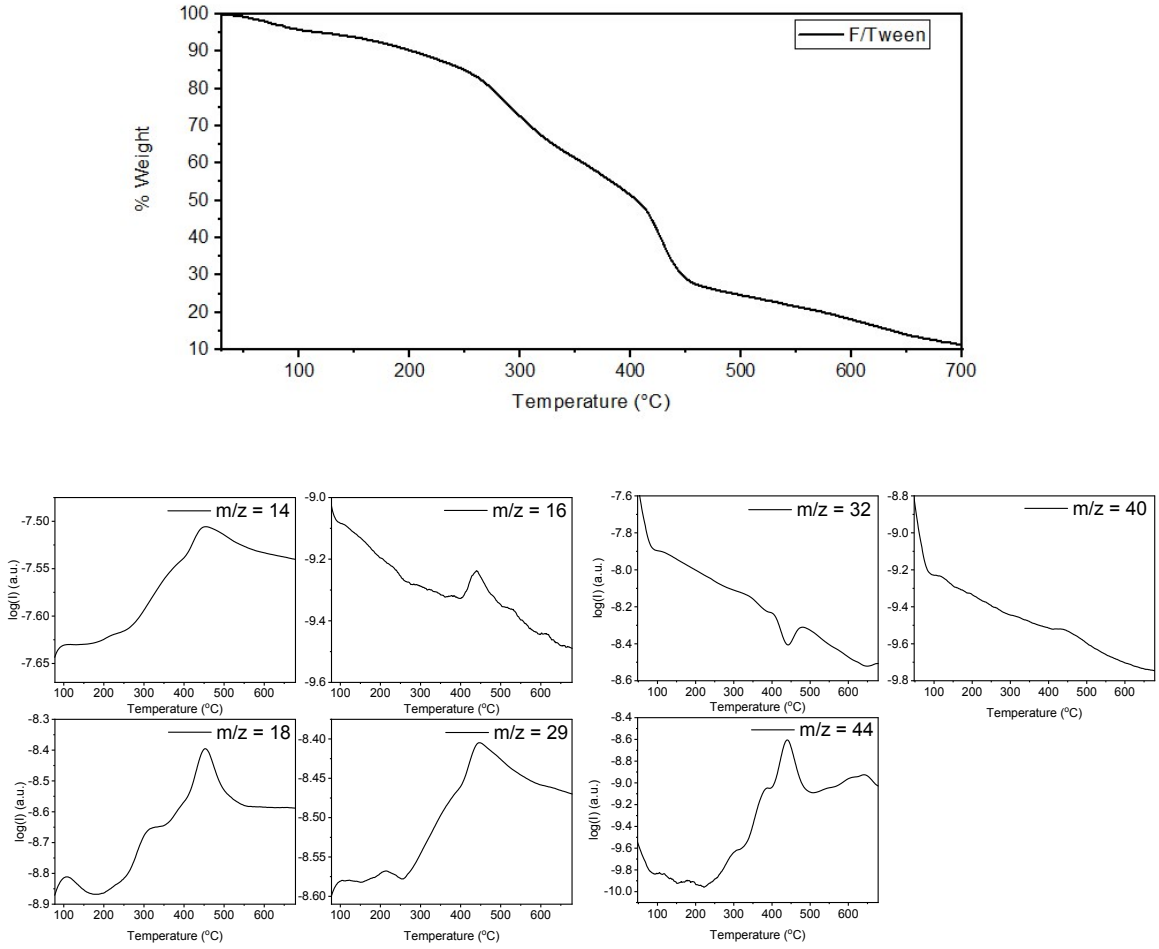

Figure S13. TGA-MS of F/Tween.

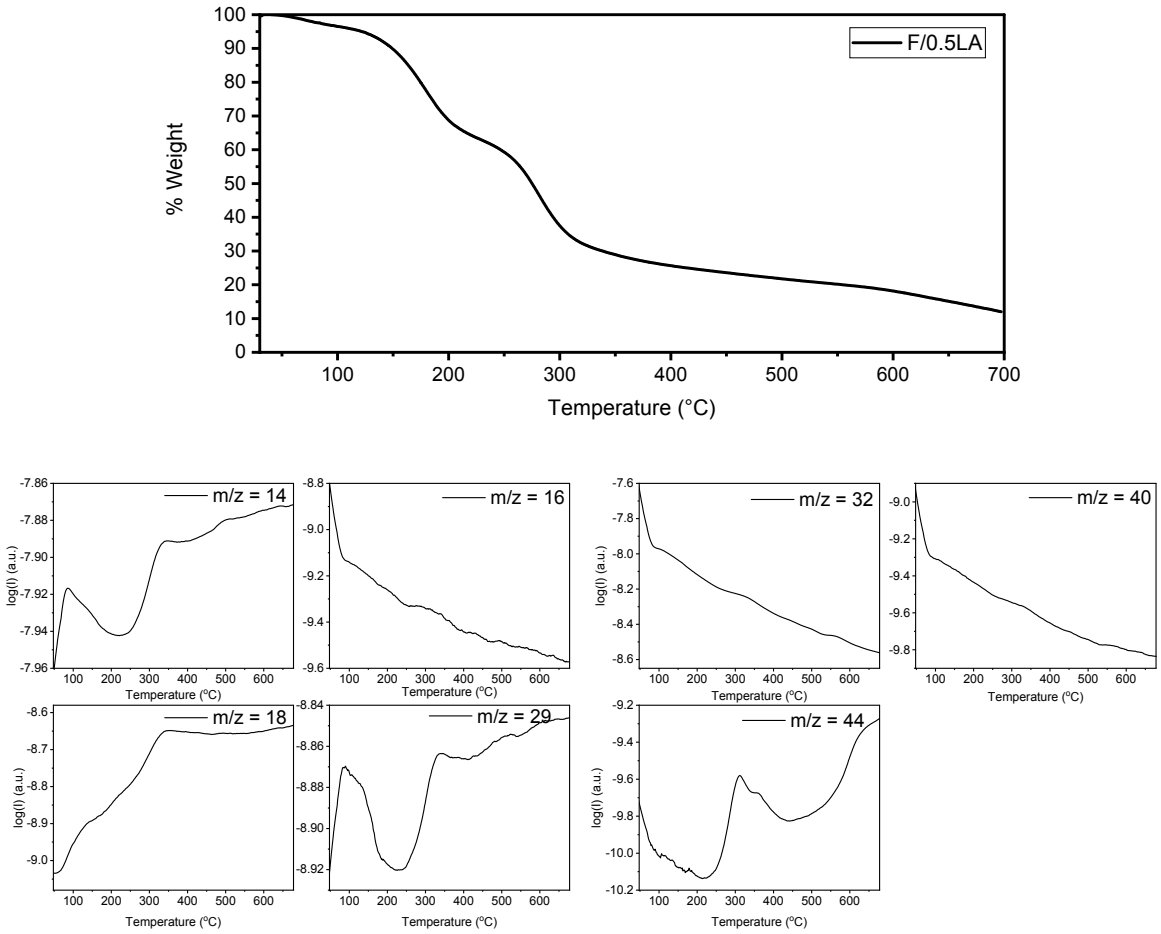

Figure S14. TGA-MS of F/0.5LA

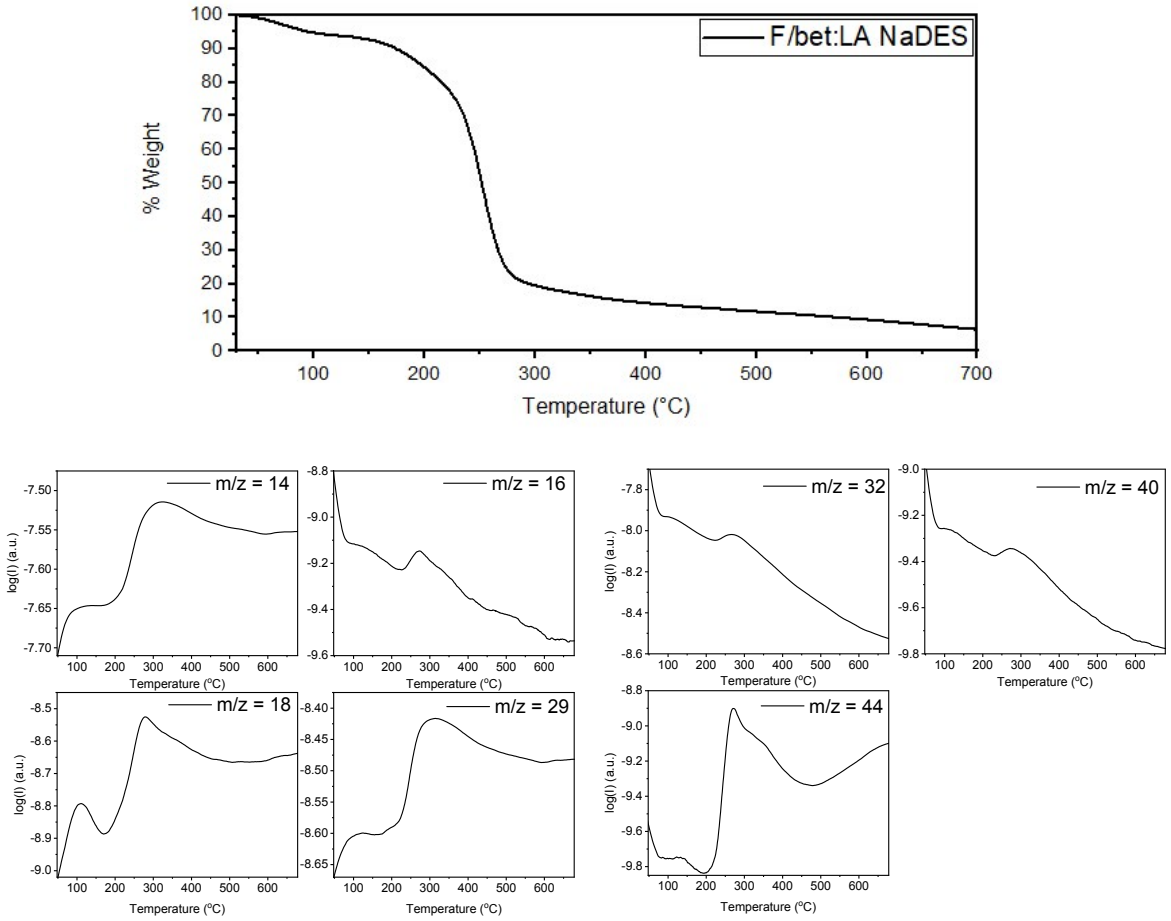

Figure S15. TGA-MS of F/bet:LA NaDES

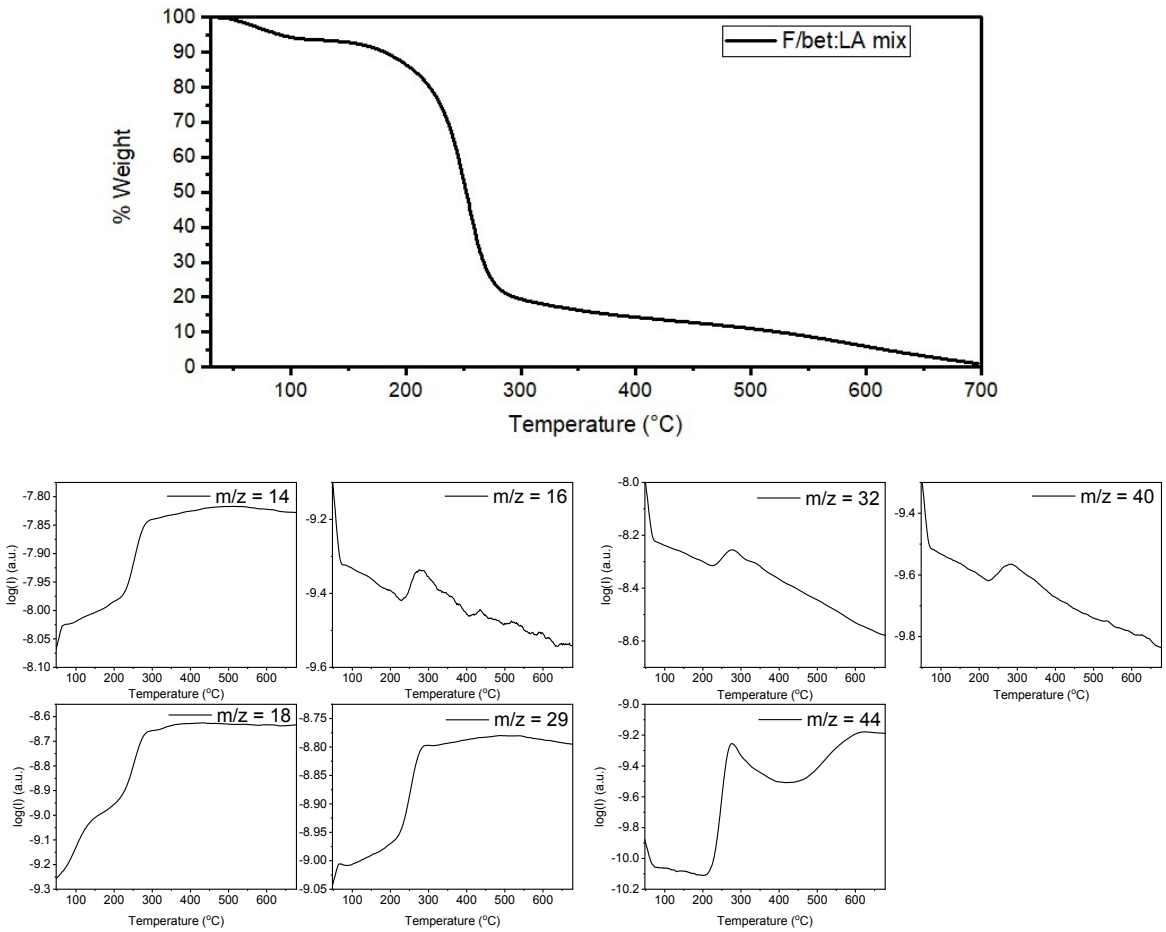

Figure S16. TGA/MS of F/bet:LA mix

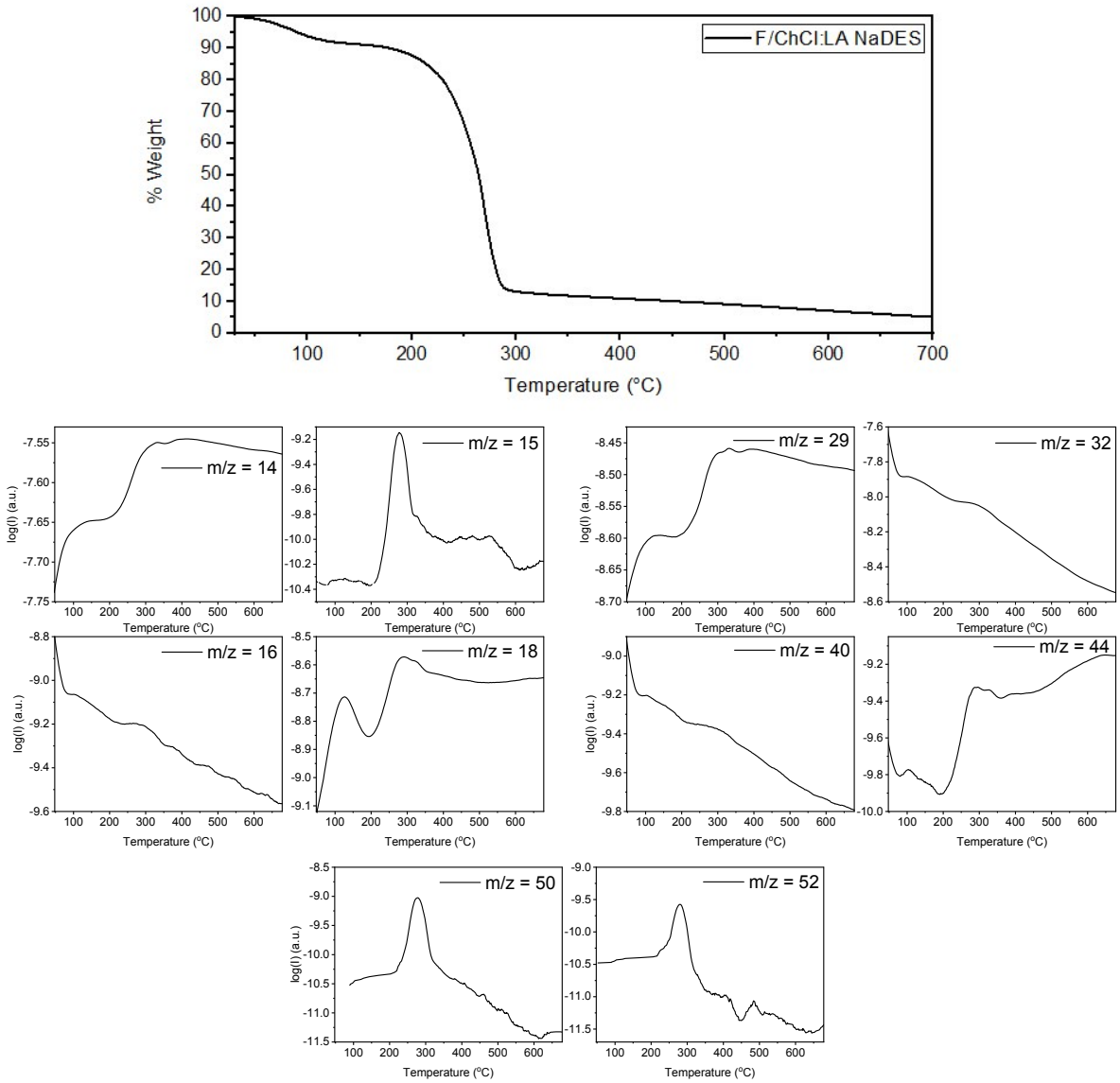

Figure S17. TGA-MS of F/ChCl:LA NaDES

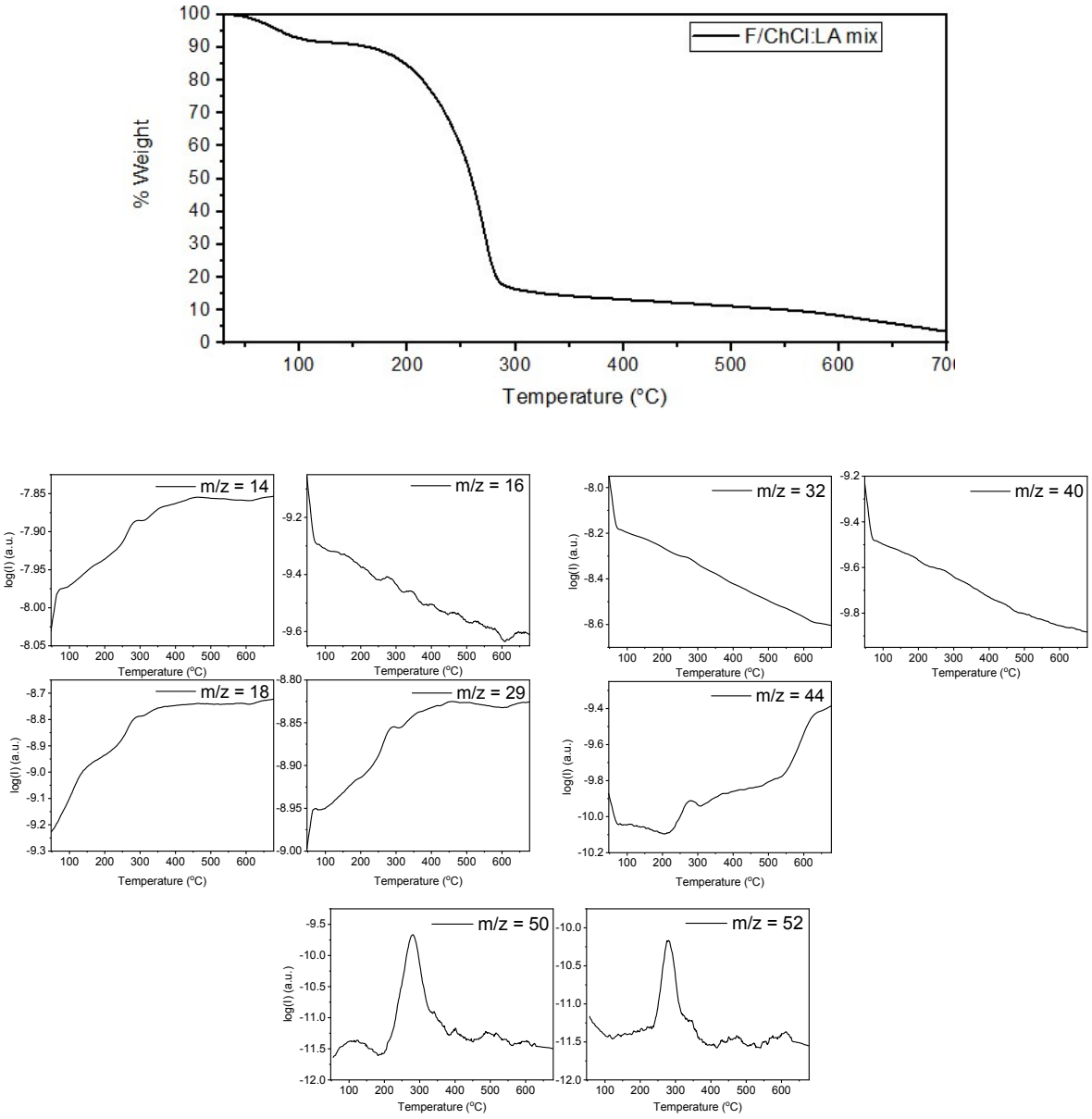

Figure S18. TGA-MS of F/ChCl:LA mix

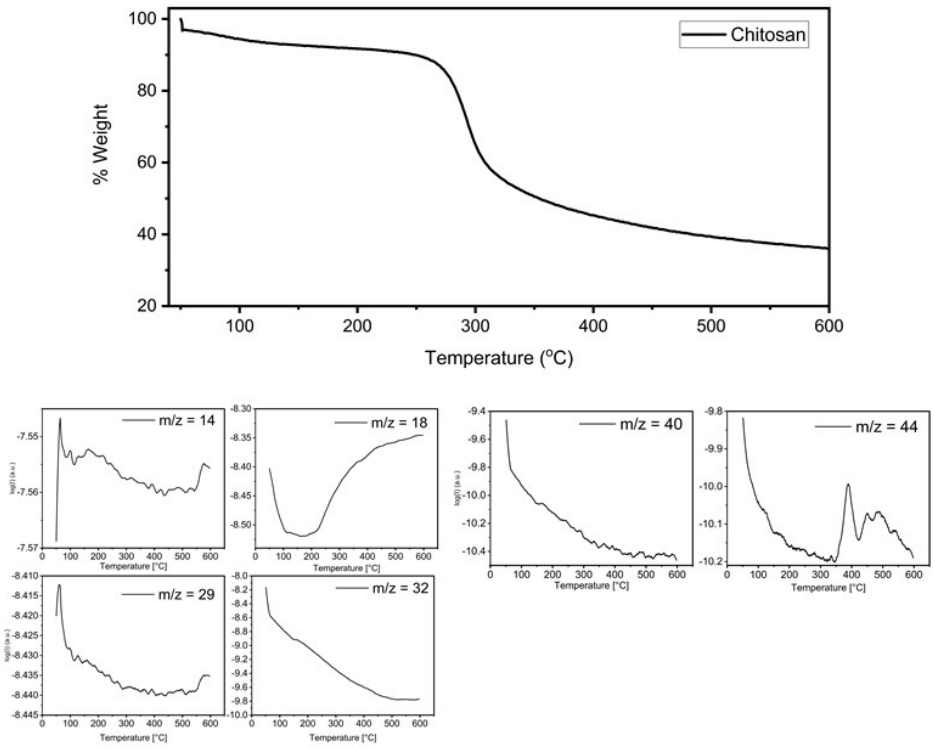

Figure S19. TGA-MS of chitosan

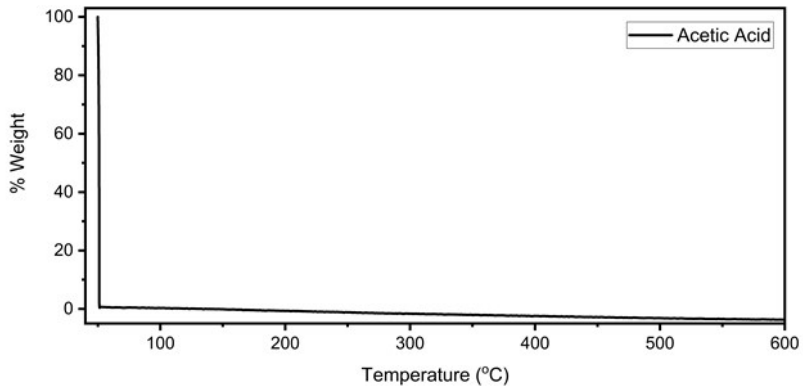

Figure S20. TGA of acetic acid.

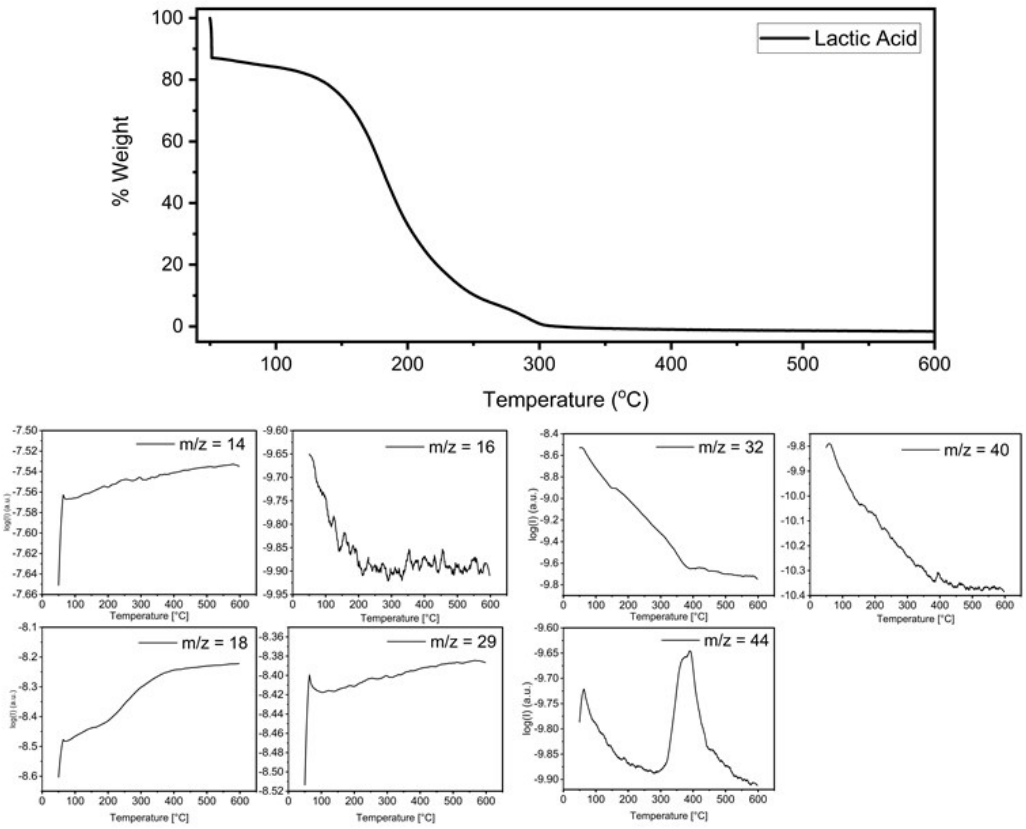

Figure S21. TGA-MS of lactic acid.

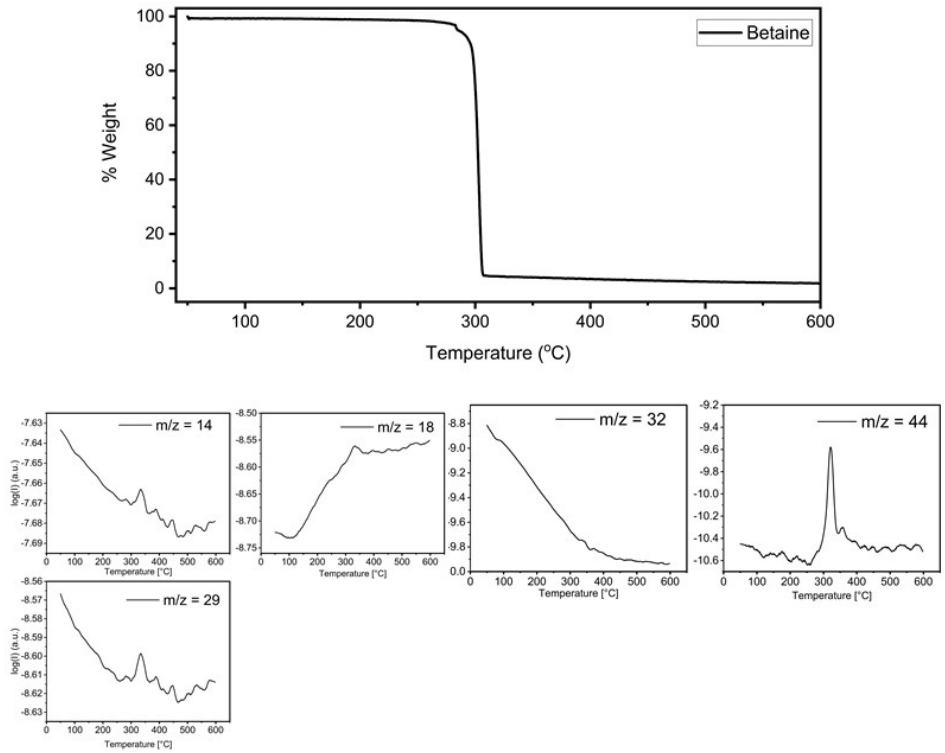

Figure S22. TGA-MS of betaine.

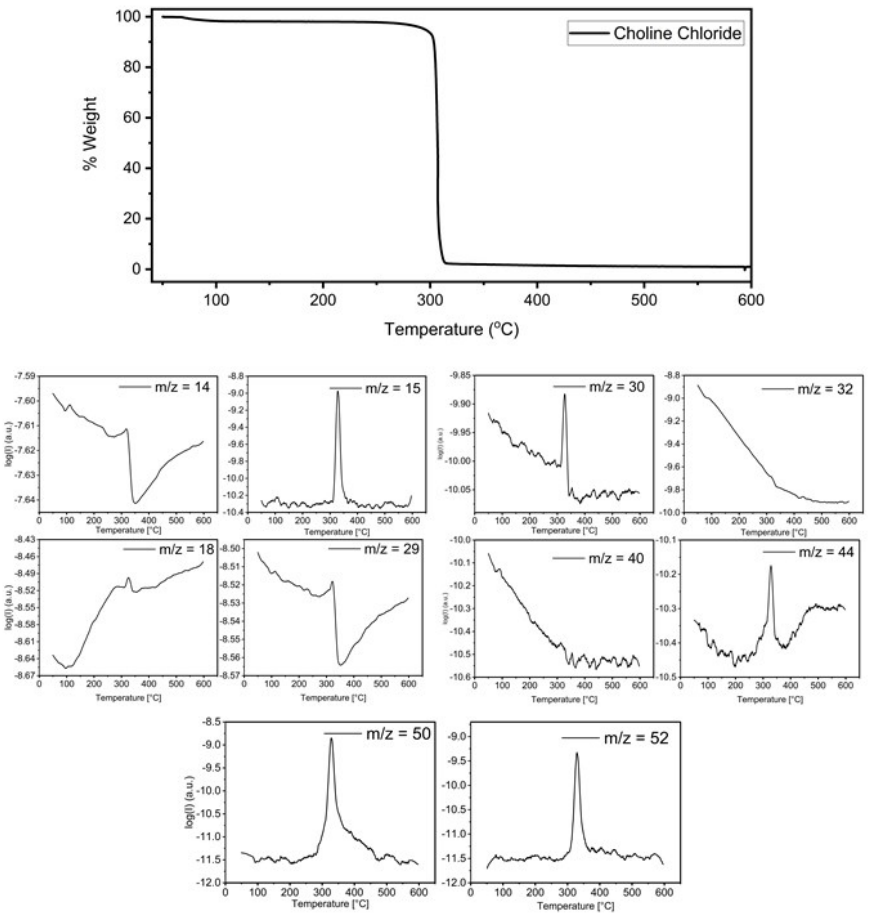

Figure S23. TGA-MS of choline chloride.